Nuclear Instruments and Methods in Physics Research A 830 (2016) 206–213

Contents lists available at ScienceDirect

Nuclear Instruments and Methods in Physics Research A

journal homepage: www.elsevier.com/locate/nima

Readout electronics validation and target detector assessment for the Neutrinos Angra experiment

T.A. Alvarenga [a], J.C. Anjos [b], G. Azzi [b], A.S. Cerqueira [a], P. Chimenti [c], J.A. Costa [a], T.I. Dornelas [a], P.C.M.A. Farias [d], G.P. Guedes [e], L.F.G. Gonzalez [f], E. Kemp [f], H.P. Lima Jr. [b], R. Machado [b], R.A. Nóbrega [a,*], I.M. Pepe [d], D.B.S. Ribeiro [a], E.F. Simas Filho [d], G.A. Valdiviesso [g], S. Wagner [h]

[a] Federal University of Juiz de Fora, Juiz de Fora-MG, Brazil
[b] Brazilian Center for Research in Physics, Rio de Janeiro-RJ, Brazil
[c] Federal University of ABC, Santo André-SP, Brazil
[d] Federal University of Bahia, Salvador-BA, Brazil
[e] State University of Feira de Santana, Feira de Santana-BA, Brazil
[f] State University of Campinas, Campinas-SP, Brazil
[g] Federal University of Alfenas, Poços de Caldas-MG, Brazil
[h] Pontifical Catholic University of Rio de Janeiro, Rio de Janeiro-RJ, Brazil

ARTICLE INFO

Article history:
Received 2 September 2015
Received in revised form
11 May 2016
Accepted 11 May 2016
Available online 24 May 2016

Keywords:
Neutrinos detector
Instrumentation
Photon detection

ABSTRACT

A compact surface detector designed to identify the inverse beta decay interaction produced by anti-neutrinos coming from near operating nuclear reactors is being developed by the Neutrinos Angra Collaboration. In this document we describe and test the detector and its readout system by means of cosmic rays acquisition. In this measurement campaign, the target detector has been equipped with 16 8-in PMTs and two scintillator paddles have been used to trigger cosmic ray events. The achieved results disclosed the main operational characteristics of the Neutrinos Angra system and have been used to assess the detector and to validate its readout system.

1. Introduction

The main purpose of the Neutrinos Angra (ν-Angra) Experiment [1,2] is to develop a compact surface detector capable of identifying interactions produced by antineutrinos coming from a nearby operating nuclear reactor. By measuring the anti-neutrinos flux, it is possible to monitor the reactor activity and to estimate the thermal power produced in the reactor core [3]. The Collaboration also intends to study the possibility of measuring the neutrinos energy spectrum variation during the burn up of the nuclear fuel, which can be used to infer the isotopic composition of the reactor fuel [4].

Compared to the usually employed underground detectors, one of the main advantages of the ν-Angra detector design comes from the fact that it is of easy deployment and operation, since it is compact and there would be no need to open underground tunnels to acquire useful data. In addition, the detector will be filled with water doped with Gadolinium (Gd) which is a non-flammable material, instead of using liquid scintillator which is used by most of the experiments of this type. Neutrinos' detection will occur by inverse beta decay ($\bar{\nu}_e + p \rightarrow n + e^+$), where the emitted positron is above the Cherenkov threshold, becoming visible to the detector as a prompt light signal and the neutron goes through a thermalization process to be then captured by a Gd nuclei which in turn emits a gamma cascade with average energy of 8 MeV. These gammas are able to release electrons from the water atoms with energy above the Cherenkov limit, generating a new light signal a few microseconds after the prompt signal. This delayed time coincidence will be used as the signature for a neutrino interaction event candidate. According to Monte Carlo (MC) simulations, approximately 4.5 k $\bar{\nu}_e$ events per day are supposed to be fully contained, leaving light pulses from both prompt (positron) and delayed (neutron) signals inside the target.

The method for neutrino's detection relies on the time correlation between these two signals, on efficient shielding and veto systems and also on an accurate knowledge of the detector and background events characteristics. For instance, two selection

* Corresponding author.
E-mail address: rafael.nobrega@ufjf.edu.br (R.A. Nóbrega).

http://dx.doi.org/10.1016/j.nima.2016.05.052
0168-9002/

rules are particularly promising: (1) selecting events that produce between 10 and 200 photoelectrons which leaves about 90% of positrons and 89% of neutrons untouched; (2) considering the time difference between the prompt and the delayed signals. In this case, 99% of the positron-neutron events have a time shift lower than 50 μs (for a 0.3% Gd concentration). The overall combined $\bar{\nu}_e$ detection efficiency may be as high as 79% while background level is dramatically reduced, i.e., muon events rate might be reduced from 350 Hz to less than 0.2 Hz after selection cuts are applied.

The ν-Angra target detector has been recently assembled with 16 8-in R5912 Hamamatsu PMTs [5,6]. In order to acquire the signals generated by cosmic ray events, a full readout chain, composed of custom front-end and acquisition electronics, has been put together with the purpose of assessing the target detector, studying background signal characteristics and validating the readout electronics. This work completes the development phase of the target detector and its instrumentation, making them ready for acquiring data nearby an operating nuclear reactor.

In Section 2 the ν-Angra detector and its readout electronics are introduced, in Section 3 the cosmic rays acquisition setup is described, in Section 4 the cosmic rays acquisition results are presented and finally in Section 5 the conclusions are pointed out.

2. The ν-Angra detector and readout system

2.1. Detector

The ν-Angra detector will be installed at the outer side of the concrete dome of the Angra II nuclear reactor, in a 40 ft high cube commercial container, placed at 30 m from the reactor core. The power plant is located near the city of Angra dos Reis, Brazil. The adopted detector design is an assembly of four subsystems: (1) two water tanks, 25 cm high, placed at the top and at the bottom of the target tank, equipped with 4 PMTs each and used as active shields and muon veto; (2) a lateral 25 cm passive water shield that helps to protect the inner parts from cosmic ray induced neutrons and low energy particles; (3) a water tank containing and surrounding the lateral walls of the target detector with a 25 cm wide layer, instrumented with 4 PMTs, one in each side of the tank, used as active shield and muon veto; (4) a central tank with an active volume of 1.34 m^3 used as the antineutrino target and instrumented with 32 PMTs, 16 on the top and 16 on the bottom sides. The target detector working principle is based on the Water Cherenkov technique and it is filled with a 0.3% gadolinium doped water, to enhance neutron capture. Hence, a total of 44 PMTs will be installed.

A representation of each volume is shown in Fig. 1 using a Geant4 model. The overall detector dimensions are (2.75 m × 2.10 m × 2.42 m) (length × width × height) and the target tank external dimensions are (1.50 m × 1.05 m × 1.39 m). The target mass will provide a neutrino interaction rate in the order of $5{\cdot}10^3$ events per day, considering a distance of 30 m to the reactor core and 4 GW reactor thermal power.

2.2. Readout electronics

The overall scheme of the readout system is shown in Fig. 2. Each detector signal is individually processed by a front-end channel. The analog signals coming out from its amplifier-shaper stage are delivered to the acquisition modules (NDAQ) to be digitized, processed and stored in a buffer while waiting for a decision signal from the first level trigger system (L1TS). Whenever an event is approved, the stored data is sent to the high level trigger system, where a more careful and time consuming decision

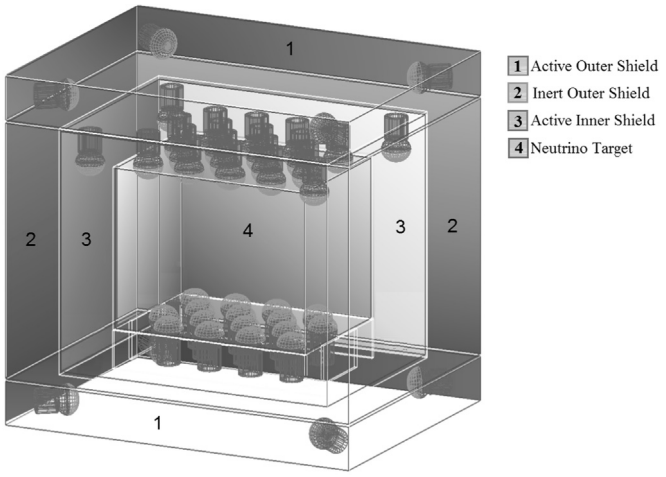

Fig. 1. Scheme of the ν-Angra detector.

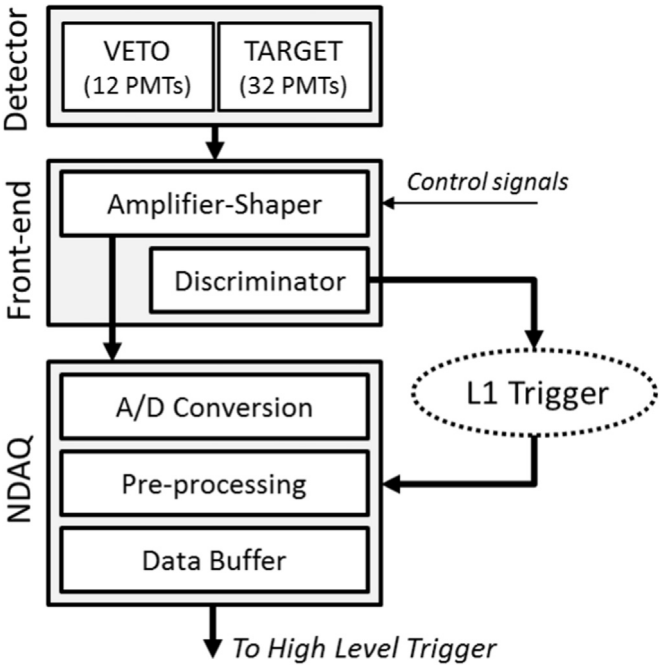

Fig. 2. Readout diagram of the ν-Angra Experiment.

is made. All the amplifier-shaper output channels, from both target and veto systems, are also connected to a discriminator circuit which, in turn, provides logic pulses to the L1TS for antineutrino candidates selection. The L1TS selection criteria are based on parameters such as time difference between the received signals, whether or not the incoming events hit the veto detectors and coincidence in time between the PMT devices signals. Additionally, the L1TS will be able to estimate the energy of each PMT signal by means of pulse width measurement which will be used to filter only those events with total energy within the expected positron-neutron energy spectrum, increasing significantly the L1TS background rejection efficiency.

The ν-Angra readout electronics is therefore composed of a front-end circuit [7] and an acquisition module named NDAQ [8]. Both are custom solutions developed by the Collaboration. The main functionalities of the former are to read and to conform the PMT signals according to the project requirements while the latter was designed to digitize and to measure the arriving time of the front-end output signal and to transfer data to a local computer after receiving the L1TS acceptance. The main front-end

requirements are listed below:

- Shaping the PMT signal to the NDAQ A/D conversion;
- Signal duration must be short enough (below 1 μs) to allow proper measurement of the time shift between positron and neutron signals;
- Relation between injected charge and output peak amplitude should be linear;
- Possibility to work with different gains must be provided. The front-end gain of the target detector channels shall be adjusted to avoid saturation of the signals generated by positron and neutron events.[1] For the veto system, the front-end gain will be adjusted to optimize its detection efficiency.
- Analog and discriminated signals must be delivered to the data acquisition and to the trigger systems, respectively.

2.2.1. Front-end module

Eight front-end modules have been produced to fully-equip the Neutrinos-Angra detector. Each module has eight channels composed of a 50 Ω input-impedance attenuator, an Amplifier-Shaper-Discriminator (ASD) and an I^2C-based circuitry, the latter makes it possible to control the discriminator threshold and the signal offset at the ASD output stage. A scheme of a front-end channel is shown in Fig. 3.

The target detector should detect and measure the energy left by the interacting neutrinos. The particles coming out from the neutrinos' interactions are expected to generate less than 10 photoelectrons/PMT, in average. Therefore, the front-end circuit has been designed to be linear up to a charge of 60 pC, which corresponds to approximately 37 photoelectrons, using a gain of 24.7 mV/pC and considering a front-end input impedance of 50 Ω [9]. An attenuator circuit has been foreseen to enable the adjustment of the overall system gain should it be required.

2.2.2. Acquisition module

A simplified block diagram of the acquisition module is presented in Fig. 4. Each analog-to-digital conversion channel is implemented using a 12-bit multi-stage pipeline ADC[2] able to sample the input signal at 125 MHz. By using 10 bits for quantization and a dynamic range of 2Vpp, a voltage resolution around 2 mV is achieved, which is expected to cover the required resolution in energy for neutrino events detection. For high-precision measurement of time between pulses, an 8-channel Time-to-Digital Converter (TDC) chip[3] has been selected. The TDC presents a resolution of 81ps and is able to measure pulses in a dynamic range of 9.8 microseconds. ADC and TDC information feed the $FPGA_{core}$,[4] where additional processing algorithms can be applied before transferring data to a local computer. The $FPGA_{vme}$[5] handles the VME data transfer which happens by means of a VMEbus single board computer.[6]

3. Cosmic rays acquisition setup

A scheme of the applied readout and trigger systems is presented in Fig. 5. The 16 PMTs signal cables were connected to the inputs of the front-end cards. The front-end output signals were sent to the NDAQ modules, where the signals are digitized and sent to a local computer through a VME controller by means of

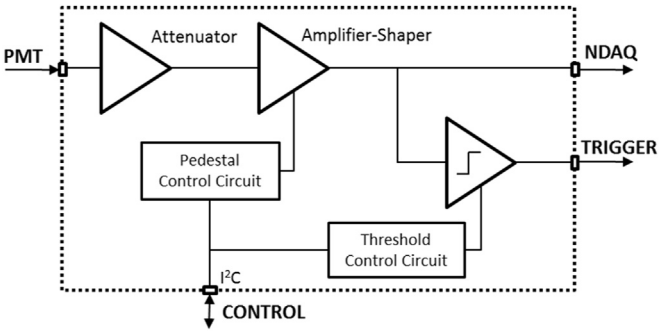

Fig. 3. Scheme of a front-end channel.

Ethernet protocol. Two scintillator paddles, with active area of 14 cm × 14 cm and 1 cm thickness, were positioned just above the detector to produce trigger information for cosmic events. Their signals were sent to a discriminator and then to a logic port configured to provide coincidence between both scintillators. The resulting signal was sent to the NDAQ trigger inputs making use of a fanout NIM module. The NDAQ modules have been configured to digitize and store 100 samples (800 ns) of the input signals each time they receive a trigger pulse; 20 samples before and 80 samples after the trigger rising edge.

A high-voltage NIM module[7] was used as power supply for the scintillator paddles applied for the trigger system. Both were supplied with a voltage value of −1450 V. This value was chosen based on a high-voltage scan performed for each one of the trigger paddles while the other one was set to a fixed HV value of −1400 V. The HV supply value was scanned from −1000 to −1800 Volts using steps of −100 Volts. For each HV value, the number or coincidences was registered, as shown in Fig. 6. A plateau region between −1400 and −1600 Volts could be identified.

3.1. Detector assembling

Fig. 7 shows, on the left, four R5912 Hamamatsu PMTs ready to be placed into the detector and on the right, 16 PMTs fully installed in the bottom of the target detector. It is also possible to observe that the detector inner walls are covered with Tyvek material [10].

After covering the inner walls with Tyvek sheets and installing the PMTs, the detector was flooded with 1370 liters of filtered water. The target detector was then covered with an endcap and a black tarp to seal and to protect the detector from external light. The PMTs' cables (signal and HV) were then routed to the control room located just a few meters from the detector. Fig. 8 shows the detector completely sealed and ready to be used.

3.2. Readout system preparation

The PMTs were characterized by Hamamatsu to operate with a gain of 10^7, for this, the recommended high-voltage values were applied. The CAEN SY4527 system was used as power supply for all the 16 installed PMTs. This system was controlled by a local computer also placed in the control room. The front-end and NDAQ modules were calibrated and each single channel was checked individually.

3.2.1. Front-end calibration

To work with a lower gain to avoid signal saturation caused by the high amplitude PMT signals generated by cosmic rays, an attenuator circuit with 50 Ω input impedance was used at the input

[1] From 1 to 35 photoelectrons per PMT based on MC simulations.
[2] AD9627, Analog Devices.
[3] TDC-GPX, acam.
[4] EP3C40F484C6, Altera.
[5] EP3C25F324C8, Altera
[6] MVME3100, Emerson Network Power.
[7] N1470, CAEN.

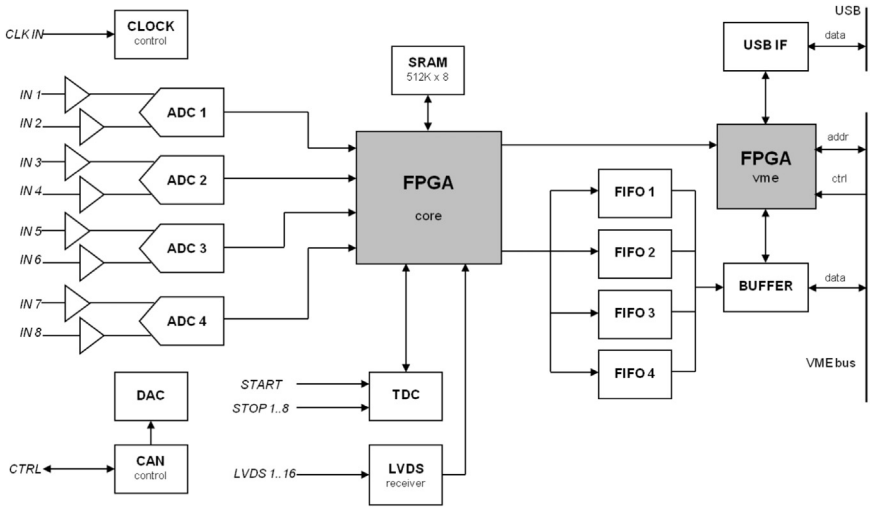

Fig. 4. Scheme of the ν-Angra acquisition electronics.

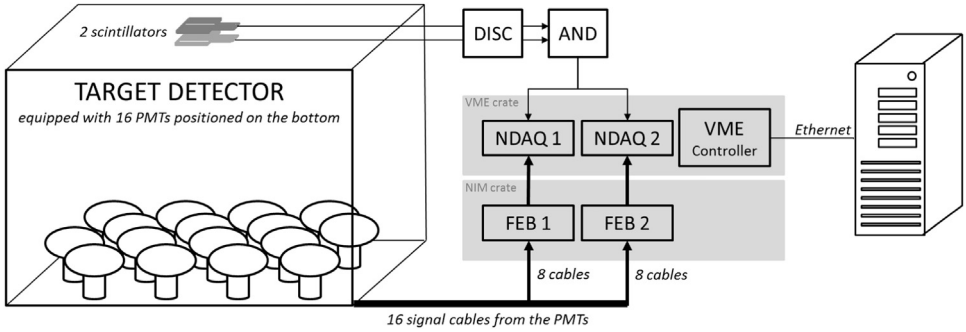

Fig. 5. Scheme of the readout system used for cosmic rays acquisition.

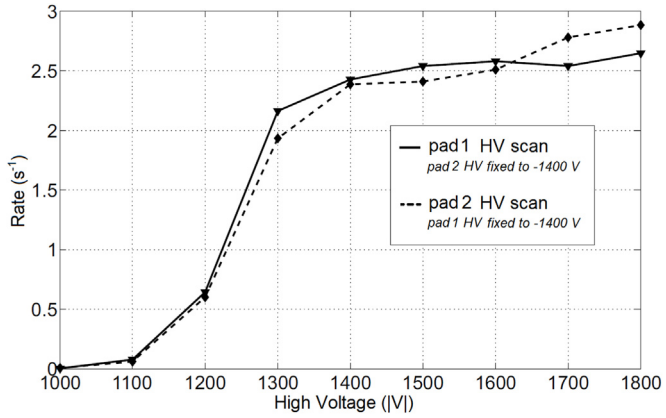

Fig. 6. High voltage (absolute value) versus coincidence rate for both trigger paddles.

of each front-end channel, reducing the signal by a factor of 10.4. Therefore, the overall front-end gain to be used during cosmic rays acquisition is approximately 2.4 mV/pC. It should be taken into account that the front-end output signal saturates approximately at an amplitude value of 1.4 V, corresponding to about 365 photoelectrons. The electronic noise standard deviation present at the front-end circuit output was estimated to be around 1 mV, which corresponds to approximately 0.25 photoelectron.

3.2.2. *NDAQ calibration*

Fig. 9 shows the calibration data obtained by injecting Gaussian shaped pulses of different amplitudes and 100 ns time duration (standard deviation), produced by a waveform generator, into every single channel of the NDAQ modules; the pulses peak values were used to build the presented plot. Only positive amplitude signals were injected, following the front-end output signal characteristics. By observing the data it was possible to conclude that both NDAQ modules were working properly, with an amplitude resolution which corresponds to an 8-bit ADC operating within a dynamic range from -1.25 V to 1.25 V (9.8 mV/ADC count).

4. Cosmic rays acquisition results

After carefully checking all the system channels, a cosmic rays acquisition has been carried out, storing 10,000 triggered events in total. Fig. 10 shows the resulting distribution of the number of fired PMTs per event considering the 16 target detector channels. As it can be seen, 35% of the triggered events did not produce any signal inside the target detector, what can be explained by the presence of dark current triggered signals (random coincidences between both scintillator paddles) and low energy electromagnetic particles [11]. Those events will produce a high rate of events with energy very close to zero. On the other hand, taking into account the cosmic events that produced at least one signal into the detector, about 75% of them fired up all the 16 PMT devices.

Fig. 11 shows the signals from the first 100 events acquired at one readout channel. As can be seen, some of the acquired signals reached the ADC saturation value, at 127 ADC counts. Fig. 12 shows, on the left side, the peak time distribution for one channel and, on the right side, for all the detector channels, in sample units. As can be seen, the amplitude peaks of the triggered signals

Fig. 7. Four PMTs on the mechanical support just before their installation inside the target detector (left) and the 16 PMTs installed on the bottom part of the target detector (right).

Fig. 8. Picture of the assembled detector, filled with water and sealed.

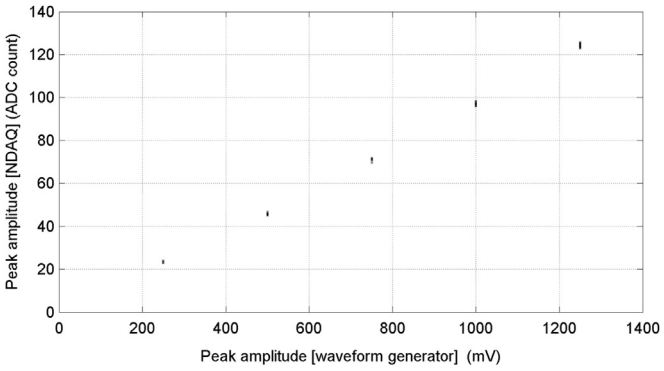

Fig. 9. Calibration data for the 16 NDAQ channels.

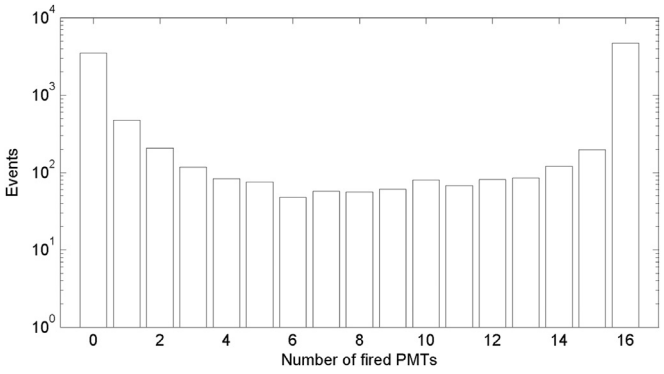

Fig. 10. Distribution of the number of coincidences.

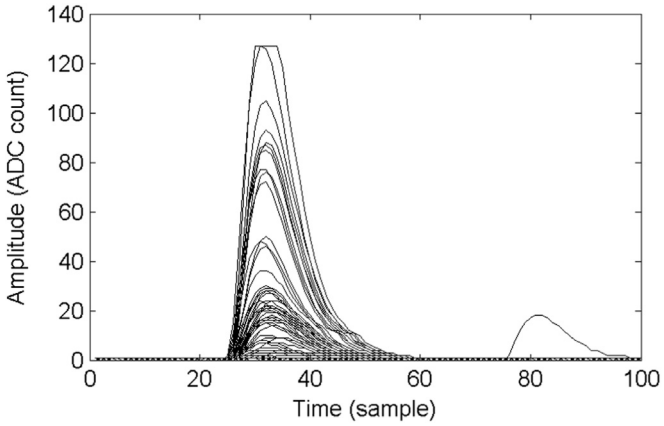

Fig. 11. Acquired pulses of the first 100 events for one readout channel.

occur around an average value of 32.18 ± 0.004 samples, with a standard deviation of 1.24 ± 0.003 samples, which is equivalent to a peak time spread of 9.9 ns. The distributions' mean and RMS values for each single channel are listed in Table 1.

About 2% of the signals have entered into the NDAQ saturation region, which occurs at 127 ADC counts (1250 mV). This effect can be seen in Fig. 13 where the peak amplitude versus the sum of sampled amplitudes of the generated signals for one detector channel is shown. A linear fit was applied to all the detector channels resulting in an average of 0.55 ± 0.025 and 0.08885 ± 0.00013 for A and B respectively according to the equation $A+Bx$; only non saturated signals were considered. The results for each single channel can be seen in Table 2. It confirms that the event charge can be inferred using either the area or the peak of the acquired signal.

As observed, 14% of the events produced a saturated signal in at least one of the 16 readout channels. Thus, the amplitude of those saturated signals must be estimated in order to allow fully reconstruction of the detector photoelectron spectrum produced by the cosmic rays particles. Those signals have been recovered by means of a χ^2-based fit algorithm using the mean shape of the front-end output signal as reference. Fig. 14 shows examples of four recovered signals for different peak amplitudes. As can be observed, signals with peak amplitude values above 180 ADC counts present a slight waveform distortion due to saturation effects, mainly on the falling edge. In those cases, a higher weight has been given to the rising edge. Nevertheless, the number of signals with peak amplitude above 180 ADC counts is small, representing only 0.4% of the total. Fig. 15 shows the peak amplitude distribution for all the 16 PMT devices, after applying the χ^2-based algorithm.

After estimating the signals peak amplitudes, those values were

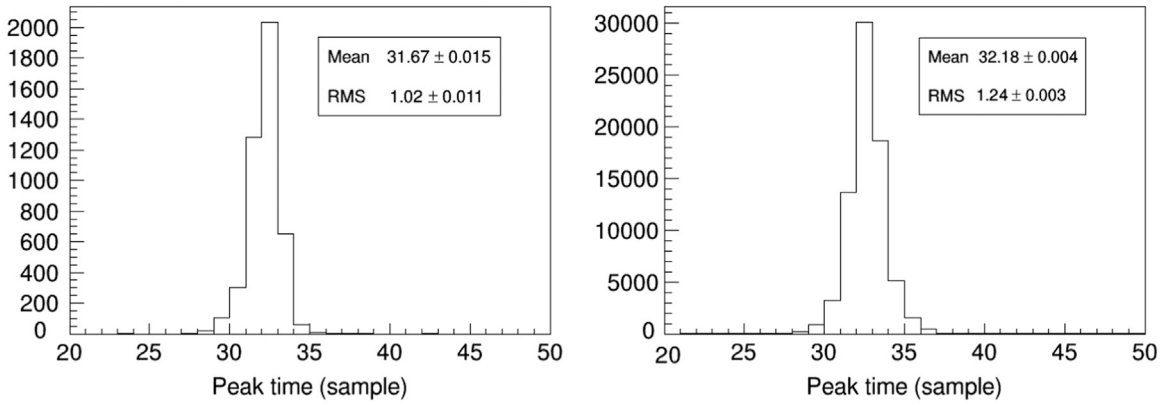

Fig. 12. Peak time distribution for channel 9 (left) and for the whole detector (right).

Table 1
Mean and RMS of the peak time distribution for each detector channel in sample units.

Ch	MEAN	RMS	Ch	MEAN	RMS
01	32.21 ± 1.5E−2	1.01 ± 1.1E−2	09	31.67 ± 1.5E−2	1.02 ± 1.1E−2
02	32.62 ± 1.5E−2	0.86 ± 1.0E−2	10	31.63 ± 1.6E−2	1.08 ± 1.1E−2
03	32.98 ± 1.7E−2	1.27 ± 1.2E−2	11	31.62 ± 1.7E−2	1.14 ± 1.2E−2
04	33.39 ± 1.6E−2	1.22 ± 1.2E−2	12	32.38 ± 1.5E−2	1.02 ± 1.1E−2
05	32.15 ± 1.5E−2	0.99 ± 1.1E−2	13	31.61 ± 1.7E−2	1.19 ± 1.2E−2
06	31.79 ± 1.4E−2	0.94 ± 1.0E−2	14	31.62 ± 1.5E−2	1.00 ± 1.1E−2
07	32.15 ± 1.4E−2	0.96 ± 1.0E−2	15	31.70 ± 1.8E−2	1.29 ± 1.2E−2
08	32.90 ± 1.5E−2	1.02 ± 1.1E−2	16	32.22 ± 1.8E−2	1.31 ± 1.3E−2

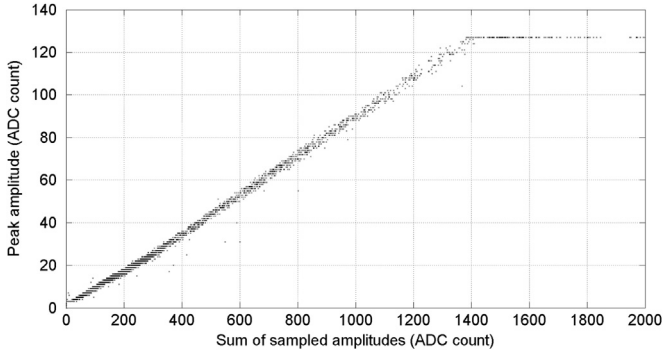

Fig. 13. Peak amplitude versus sum of the sampled amplitudes for channel 4.

converted into number of photoelectrons, according to Section 3.2. A clear picture of the channels' photoelectron distributions could be observed. Fig. 16 shows these distributions for two detector channels.

Table 3 shows the distribution's mean value for each channel. The measured values vary from 37.9 ± 0.8 to 53.6 ± 1.0 photoelectrons. Apart from the statistical fluctuation, two other factors can justify this variation: a small overall gain difference between channels and the PMT position inside the detector. The overall mean value is 45.0 ± 3.4 photoelectrons. Normalizing by this value, it is possible to estimate a gain variation of 12% (standard deviation) between the detector channels. If only PMTs in symmetrical positions are considered, which happens in pairs, this value goes to 7%.

By summing the number of photoelectron for the 16 readout channels, event by event, it was possible to reconstruct the photoelectron spectrum as measured by the target detector, as shown in Fig. 17. The photoelectron distribution can be described mainly by a Landau peak, attributed to through-going muons, together with an exponential background drop caused by low energy electromagnetic particles [11]. Fig. 17 shows also the simulated photoelectron spectrum produced by muon particles, which is in good agreement with real data concerning the muon energy distribution peak. This result indicates the proper operation and calibration of the detector and its readout system. The difference between both spectra is expected since low energy electromagnetic particles, which may have also triggered the data acquisition setup, have not been considered in the simulation.

5. Conclusions

A compact surface detector has recently been assembled and dressed with 16 PMTs by the ν-Angra Collaboration. In order to equip its readout channels, a set of front-end and acquisition custom modules has been integrated with the purpose of assessing a full readout chain of the detector and to measure some of its main operational characteristics. This document presented in

Table 2
Linear parameters estimation for each detector channel (A+Bx).

Ch	A	B	Ch	A	B
01	0.372 ± 6.2E−3	0.09126 ± 2.6E−5	09	0.895 ± 6.3E−3	0.08781 ± 2.7E−5
02	0.413 ± 6.2E−3	0.09164 ± 3.3E−5	10	0.712 ± 6.3E−3	0.08791 ± 3.6E−5
03	0.480 ± 6.2E−3	0.08958 ± 3.0E−5	11	0.407 ± 6.3E−3	0.08874 ± 3.9E−5
04	0.403 ± 6.2E−3	0.08986 ± 2.7E−5	12	0.865 ± 6.4E−3	0.08650 ± 2.9E−5
05	0.409 ± 6.3E−3	0.08973 ± 3.4E−5	13	0.363 ± 6.3E−3	0.08871 ± 3.0E−5
06	0.406 ± 6.3E−3	0.09034 ± 3.5E−5	14	0.414 ± 6.4E−3	0.08859 ± 3.1E−5
07	0.392 ± 6.2E−3	0.08921 ± 3.3E−5	15	0.940 ± 6.4E−3	0.08573 ± 3.2E−5
08	0.438 ± 6.1E−3	0.08950 ± 3.0E−5	16	0.944 ± 6.2E−3	0.08662 ± 3.4E−5

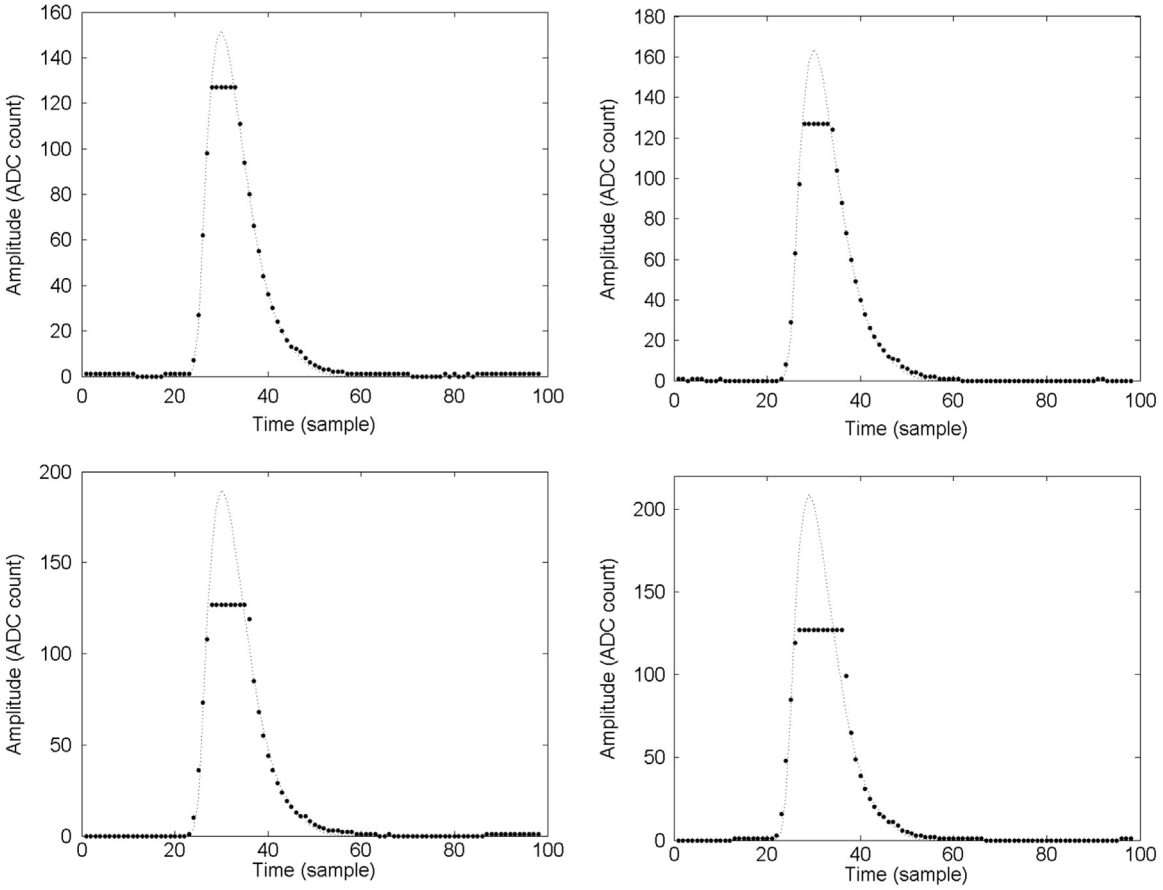

Fig. 14. Examples of saturated reconstructed signals based on a χ^2-based fit algorithm. Data points represent the measured data and dashed line the resulting fit.

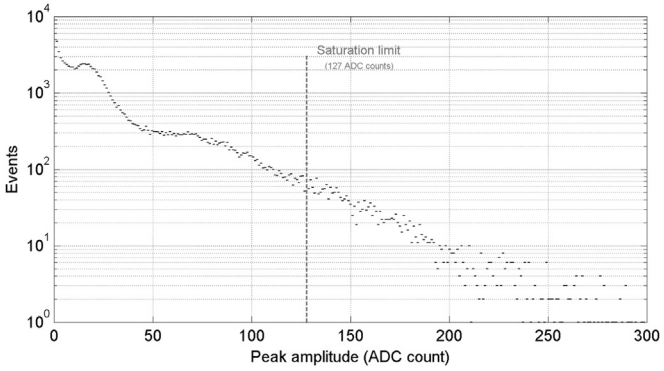

Fig. 15. Peak amplitude distribution considering all the detector channels. The peak amplitudes above 127 ADC counts were reconstructed by the χ^2-based fit algorithm.

Table 3
Photoelectrons distribution mean value for each detector channel.

PMT	MEAN	PMT	MEAN
01	51.6 ± 1.0	09	40.7 ± 0.8
02	43.0 ± 0.8	10	52.2 ± 0.9
03	42.5 ± 0.8	11	52.2 ± 0.9
04	41.8 ± 0.8	12	47.0 ± 0.8
05	44.9 ± 0.9	13	53.6 ± 1.0
06	45.1 ± 0.9	14	37.9 ± 0.8
07	40.2 ± 0.8	15	40.0 ± 0.8
08	38.3 ± 0.8	16	48.6 ± 0.9

detail the detector modules measurements required to achieve the proposed goals, successfully validating the readout system and providing an indication, by means of the observed muon spectrum, of the proper operation of the target detector.

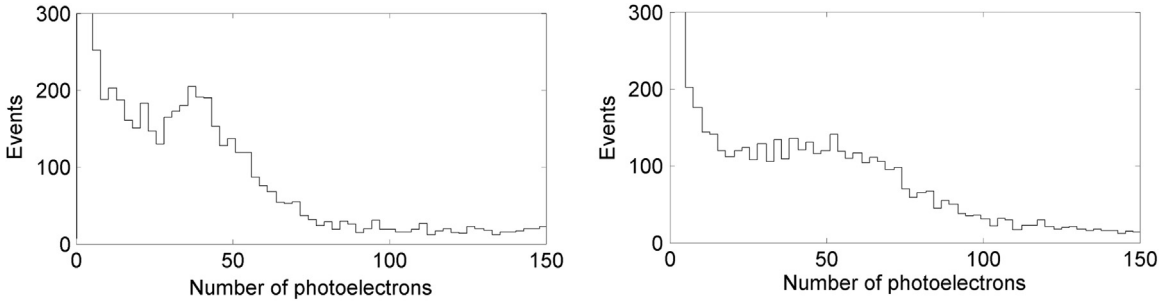

Fig. 16. Photoelectrons distribution for two readout channels: 9 (left) and 10 (right).

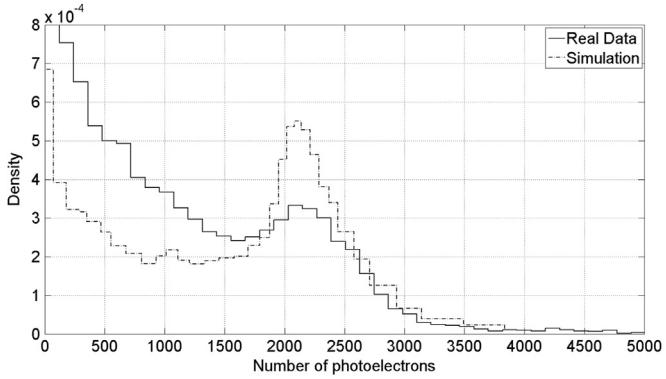

Fig. 17. Photoelectrons distribution normalized by area from experimental and simulated data.

Acknowledgement

This work was supported by several agencies, through a number of funding projects. The Angra Collaboration acknowledges the support from MCTI, CNPq, FINEP and the following state research agencies: FAPESP, FAPEMIG and FAPERJ.

References

[1] J.C. Anjos, et al., Status and perspectives of the neutrino Angra Project, in: NuInt12: Eighth International Workshop on Neutrino-Nucleus Interactions in the Few-GeV Region, Rio de Janeiro, Brazil, 2012.
[2] J.C. Anjos, et al., Using neutrinos to monitor nuclear reactors: the Angra neutrino experiment, Simul. Detect. Status Nucl. Phys. B Proc. Suppl. (2015) 1–8.
[3] N.S. Bowden, et al., Observation of the isotopic evolution of pressurized water reactor fuel using an antineutrino detector, J. Appl. Phys. 105 (2009) 064902.
[4] Th.A. Mueller, et al., Phys. Rev. C83 (2011) 054615.
[5] Hamamatsu Catalog, Large Photocathode Area PMTs, Catalog No. TPMH1286E05, 2008.
[6] S.J. Bricea, et al., Photomultiplier tubes in the MiniBooNE experiment, Nucl. Instrum. Methods Phys. Res. Sect. A 562 (2006) 97–109.
[7] J.A. Costa, T.I. Dornelas, R.A. Nóbrega, A.S. Cerqueira, Front-end electronics of the Neutrinos Angra Project, in: Proceedings of IEEE Instrumentation and Measurement Technology Conference (I2MTC 2014), Montevideo, Uruguay, 2014.
[8] H.P. Lima Junior, et al., Data acquisition with optimal pulse amplitude estimation for a neutrino detection experiment, Technical Note, vol. 4, no. 2, pp. 34–41, Brazilian Center for Research in Physics, 2014.
[9] T.I. Dornelas, Estudo, Desenvolvimento e Análise da Instrumentação do Experimento Neutrinos Angra [Study, Development and Analysis of the Neutrinos Angra Experiment Instrumentation] (Master thesis), Federal University of Juiz de Fora, February 2015.
[10] J.C. Arteaga-Vellzquez, C. Vlzquez-Lpez, A. Zepeda, A measurement of the diffuse reflectivity of 1056 Tyvek in air and water, Nucl. Instrum. Methods Phys. Res. Sect. A: Accel. Spectrom. Detect. Assoc. Equip. 553 (1–2) (2005).
[11] P. Billoir, The Cherenkov surface detector of the Pierre Auger observatory, Nucl. Instrum. Methods Phys. Res. Sect. A 766 (2014) 78–82.